FPRS WOOD AWARD PAPERS

SENARMONT COMPENSATION FOR DETERMINING FIBRIL ANGLES OF CELL WALL LAYERS

TENSION WOOD ANATOMY OF SILVER MAPLE

By

Floyd G. Manwiller

Forest Products Journal, vol. 16, No. 10, pp. 26-30. October 1966.

and

Forest Products Journal, vol. 17, No. 1, pp. 43-48. January 1967

Wood Award Winner

Senarmont Compensation for Determining Fibril Angles of Cell Wall Layers

By

F. G. Manwiller

Southern Forest Experiment Station
Alexandria, La.

Abstract

A technique originated by Preston, is explained for determining fibril angles of the secondary wall layers of fibers. A polarizing microscope equipped with Senarmont compensator is used to measure birefringence of the wall layers in a series of sections cut at various angles to the long axis of the cells. Enough measurements are taken on each section to give a representative average. A plot of birefringence against section angle for each layer defines a curve. Fibril angle in the layer is estimated equal to the section angle corresponding to the maximum of this curve.

THE WALL OF A TYPICAL wood fiber consists of a primary wall and a secondary wall of three layers: the outer S_1, the central S_2, and the inner S_3. The layers consist of systems of helically wound microfibrils. This paper discusses a technique for measuring the steepness and direction of winding of the helix within any one layer. The technique, which requires a polarizing microscope equipped with a Senarmont compensator, was developed by Preston in 1952[2] but has not been fully described in print. The following discussion is based on books by Johannsen,[3] Preston,[2] and Wahlstrom,[4] on personal communication with Preston, and on Mark's work[5].

The technique permits fibril angle estimations based on large numbers of measurements for all layers in the fiber. Conventional microscopy measures the S_2 layer only, and with the electron microscope, sectioning difficulties preclude large numbers of observations on individual layers.

Optical Aspects of Cell Wall Structure

The polarizing microscope is optically similar to a simple compound microscope except that it contains a polarizer below the condenser and an analyzer between the objective and the eyepiece. The elements are crystals that transmit light vibrating in one plane only (light travels with simple harmonic wave motion). When the vibration directions of the polarizer and analyzer are at right angles to each other, no light reaches the observer.

[1]The research was conducted while the author was Research Associate at Iowa State University. Journal Paper No. J-5429 of the Iowa Agriculture and Home Economics Experiment Station, Ames, Iowa, Project 1583.

[2]Preston, R. D. 1952. The molecular architecture of plant cell walls. New York: John Wiley and Sons, Inc.

[3]Johannsen, A. 1918. Manual of petrographic methods. Ed. 2, New York: McGraw-Hill Book Co.

[4]Wahlstrom, E. E. 1960. Optical crystallography. Ed. 3, New York: John Wiley and Sons, Inc.

methods. Ed. 2. New York: McGraw-Hill Book Co.

[5]Mark, R. 1965. Tensile stress analysis of the cell walls of coniferous tracheids. In Cote, W. A., Jr., ed. Cellular ultrastructure of woody plants, pp. 493 — 533. Syracuse, New York: Syracuse Univ. Press.

This paper won first place in the 1966 Wood Award Competition, co-sponsored by the Forest Products Research Society and Wood and Wood Products magazine. It was presented at Session 10 — Anatomy and Fundamental Properties — of the 20th Annual Meeting of the Forest Products Research Society, July 20, 1966, in Minneapolis, Minn.

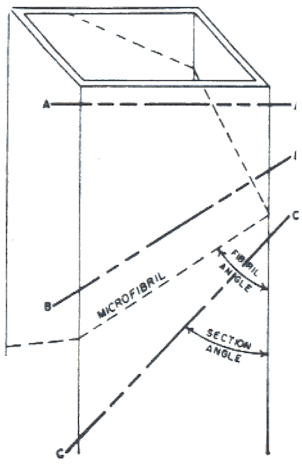

Figure 1. — Cell wall layer with microfibrils in a Z helix.

Crystalline solids optically change the light passing through them; isotropic materials do not. Wood is crystalline; it is comprised of ordered repetitive units, the microfibrils. The microfibrils have a high degree of parallelism within the lamellae of the cell wall layers. When plane-polarized light from the polarizer strikes the crystalline cell wall, it travels unchanged in one direction only — the optic axis, which is parallel to the longitudinal axis of the microfibril. If the light strikes the wall layer in any direction other than parallel to the optic axis, it is split into two rays vibrating in mutually perpendicular directions.

The interaction of light and matter can be expressed by the index of refraction (n), which can be calculated (among other ways) by dividing the velocity of light in air by its velocity in the material under consideration. The difference between the refractive indices of the two perpendicular rays is referred to as the birefringence. One ray, termed the ordinary or *O* ray, vibrates at right angles to the optic axis regardless of how the incident light strikes the specimen, and its refractive index (n_o) has a constant value. The other ray, the extraordinary or *E* ray, vibrates in the plane of the optic axis and at an angle to it, depending on the angle at which the incident beam strikes the specimen. Its refractive index (n_E) varies, and reaches its maximum in wood when the incident light is perpendicular to the optic axis. The incident light is then also perpendicular to the longitudinal axis of the microfibrils, and the birefringence ($n_E - n_o$) is maximum.

If, in a cell wall layer, the microfibrils spiral upward to the right in the wall nearest the observer, the helix is termed a *Z* helix, and if upward to the left, an *S* helix. Helix steepness is measured in terms of the fibril angle (Figure 1), the angle between the microfibrils and the cell's longitudinal axis.

If, in a cell of *Z* helix, as diagrammed in Figure 1, sections were cut along planes *A*, *B*, and *C*, and birefringence were measured in the wall nearest the observer, section *B* would have the highest birefringence since it is parallel to the orientation of the microfibrils. When the angle which each section makes with the fiber's longitudinal axis is measured and the birefringence plotted against that angle, a curve is obtained. The curve's peak, the maximum birefringence, indicates the angle of the section parallel to the fibrillar orientation and therefore the fibril angle. If birefringence were measured in the rear wall, none of the sections would be parallel with the microfibrils, and the birefringence curve would have no peak[5]. Section *B* would be parallel to the microfibrils in the rear wall if the microfibrils were wound in an *S* helix.

These optical phenomena can be used to identify the cell wall layers. When a transverse section of wood is viewed between crossed polarizer and analyzer, the isotropic intercellular substance appears dark. The primary and S_1 layers both appear bright (and indistinguishable from each other) since they are viewed at a great angle to their respective optic axes. The S_3 layer is much darker, because it is viewed more nearly parallel to the optic axes of its microfibrils. On the lumen side of the S_3 is the adjacent bright S_2. Finally, the gelatinous (*G*) layer of tension wood cells, if present, appears dark.

Whether a cell wall layer has a *Z* or *S* helix may be determined by plotting birefringence against section angle for two opposing walls[5]. Figure 2 shows such curves for the radial wall layers of silver maple fibers. The curve for the S_3 layer has a computed peak[5] at approximately 12° in the wall nearest the observer but none in the rear wall, indicating a *Z* helical arrangement of the microfibrils.

The curve for the S_1 layer has a computed peak at about 44° in the near wall, and the S_3 layer has a peak at 20°. Each curve again has a peak in the far wall, the S_1 at about 38° and the S_3 somewhere between 0° and 18°. Peaks in the curves for both walls indicate a crossed fibrillar arrangement of both *S* and *Z* helices.

To determine the average fibril angle of a cell wall layer, one must obtain birefringence values. The Senarmont compensator[5] makes it possible to measure phase differences between the specimen *O* and *E* rays and then calculate birefringence.

The polarizer and analyzer are crossed in the microscope to give extinction, and the specimen is oriented with its directions of vibration at 45° to those of the polarizer and analyzer (Figure 3). The plane-polarized light waves from the polarizer

[5]Manwiller, F. G. 1966. Tension wood anatomy of silver maple. For. Prod. Jour. In press.

are divided by the specimen into two mutually perpendicular rays of equal amplitude. They acquire a phase difference by passing through the specimen. The magnitude of the difference depends on the difference in refractive indices and specimen thickness.

To understand the following explanation, the relation of path difference to phase difference must be kept in mind. Consider a circle with diameter *AB* (Figure 4). A beam of plane-polarized light traveling perpendicular to the plane of the paper is represented by a point *N* vibrating with simple harmonic motion between *A* and *B*. From a point *P* on the circle, a line *PN* is drawn perpendicular to *AB*. As *P* moves around the circle with constant angular velocity, ω, point *N* travels along *AB* and back with simple harmonic motion, similar to that of a light wave.

Let the point reach P_1 (Figure 5) at time t_1 and P_2 at time t_2. The path difference is represented by N_1N_2. The corresponding phase differnce is $\omega(t_2-t_1) = \phi$. The distance *BAB* represents a path length of λ, i.e., the wave length of the monochromatic light used. Therefore, a phase difference of 2π (one revolution of *P*) represents a path difference of λ.

The velocities of the two waves in the specimen are dependent on their respective refractive indices.

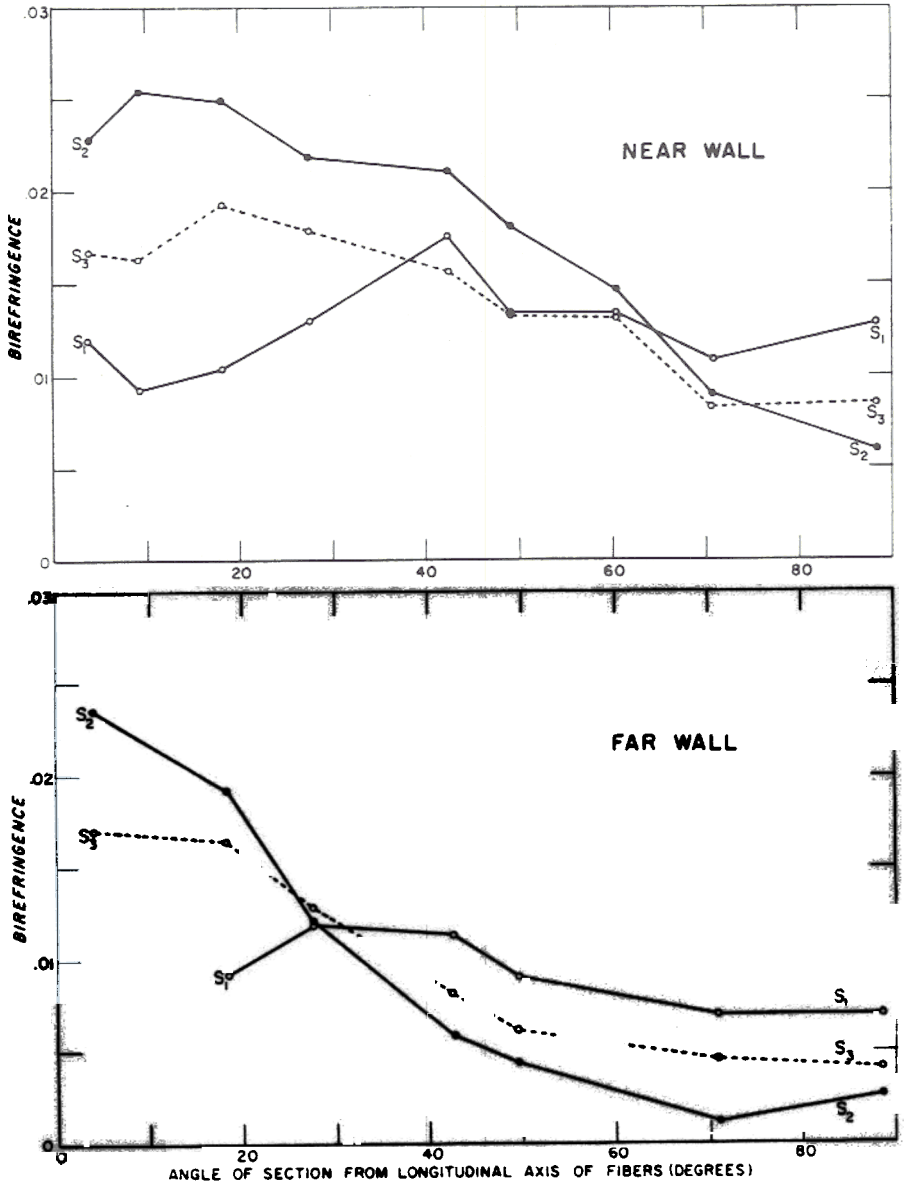

Figure 2. — Birefringence plotted against section angle for cell wall layers of radial wall nearest observer (top) and farthest from observer (bottom). Each point represents the average of one observation of each of 20 cells.

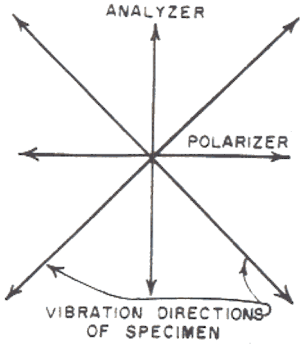

Figure 3. — Orientation of specimen with respect to polarizer and analyzer in polarizing microscope.

Let t_e be the time for the slow ray to pass through the specimen and t_o the time for the fast ray. Then if d is the specimen thickness,

$$t_e = n_e d$$

$$t_o = n_o d$$

and $$t_e - t_o = d\,(n_e - n_o),$$

the path difference. Since $2\pi = \lambda$, a path difference of $(n_e - n_o)d$ corresponds to a phase difference of $(n_e - n_o)\,(d)\,\dfrac{2\pi}{\lambda}$

When the two rays leave the specimen, they interfere to produce elliptically polarized light (as depicted by *A*, *B*, and *E* in Figure 6) whose axes, rotated 45° to those of the specimen, are parallel to those of the polarizer and analyzer. The same elliptical vibration would result from two rays that differ from each other in amplitudes (depicted by circle radius) of $a/2$ and $b/2$ and have a constant phase difference of 90° (*C*, *D*, and *E* in Figure 6). A plane-polarized vibration results when two rays differ in phase by 0° or 180°. If the elliptical vibration is considered to be formed by components with a phase difference of 90°, it can be transformed into a linear vibration by adding or subtracting a phase difference of 90° to produce the required difference of 0° or 180°. The Senarmont compensator, a crystal plate with a path difference of $\lambda/4$, (a phase difference of 90°) accomplishes this. When its vibration directions are aligned with those of the elliptical light produced by the specimen, it separates the light into two rays with a phase difference of 90° and then either increases or decreases this difference by 90°. If the fast ray of the ellipse is oriented parallel to the slow ray of the compensator, the phase difference becomes zero. A fast-ray-to-fast-ray orientation produces a phase difference of 180°. Thus plane-polarized light emerges from the compensator.

Let *AB* and *CD* (Figure 7) represent the axes of the compensator, with *CD* the direction of the slow ray. Suppose that the vibrations of the two separated rays are in phase and represented by *XX* and *YY*. If, at any time, the point moving along *XX* is at 1, that along *YY* must be at 1', and the resultant point is *L*. The resultant light emerging from the compensator is therefore plane-polarized parallel to *CD*.

The two vibrations in a cell wall layer, however, have a phase difference between them. If the layer's fast (*O*) ray is parallel to *XX* (45° counterclockwise from the fast ray of the compensator), then when the vibration along *XX* is at 1, the layer's slow vibration along *YY* will be at some point, say 2', with a phase difference of ϕ. The combination of 1 and 3' is a point *L'*, halfway between 3' and 1. The resulting plane-polarized ray is therefore *MN* at an angular distance $\phi/2$ from *CD*. The analyzer (*AB*) would be rotated counterclockwise through α to reach minimum intensity. If, on the other hand, the fast component of the specimen were oriented 45° clockwise to that of the compensator (parallel to *YY*), the analyzer would be rotated clockwise to reach minimum intensity. Clearly, $\alpha = \phi/2$ (Figure 7), and the previous equation becomes

$$2\alpha = (n_e - n_o)\,(d)\,\frac{2\pi}{\lambda}$$

and the birefringence, $n_e - n_o = \dfrac{\alpha\lambda}{\pi d}$ λ and d are in microns. Therefore,

$$n_e - n_o = \frac{(\alpha \text{ degrees})\ \ (\lambda \text{ microns})}{(3.1416 \text{ radians})\ \ (57.2956 \text{ deg/rad})\ \ (d \text{ microns})}$$

In the author's work a filter was used with a regular tungsten light source to produce a wavelength of 0.546 micron. The above equation reduces to

$$\text{Birefringence} = \frac{\alpha\ (0.003083)}{d}$$

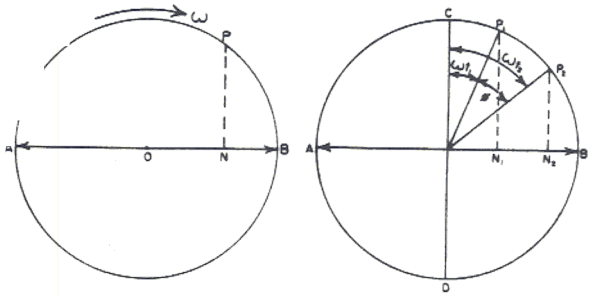

Figures 4 and 5. — Figure 4 (left) shows the simple harmonic motion of light vibration. Figure 5 (right) demonstrates the relationship of path difference to phase difference.

Using the Compensator

In measuring fibril angles in either radial or tangential walls, a series of sections similar to *A*, *B*, and *C* of Figure 1 are cut at approximately 10° intervals between transverse and longitudinal. The section angle must be accurately known to plot the birefringence curve. It may be determined by removing a longitudinal slice from the side of the sectioning block and examining it under a microscope equipped with an angle-measuring eyepiece. The layer helix direction will determine whether measurements are made on the near or the far wall.

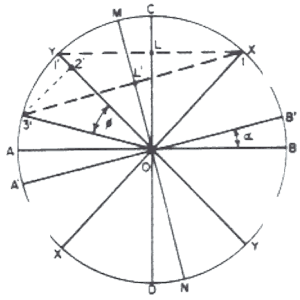

Figure 7. — Graphic development of analyzer rotation angle.

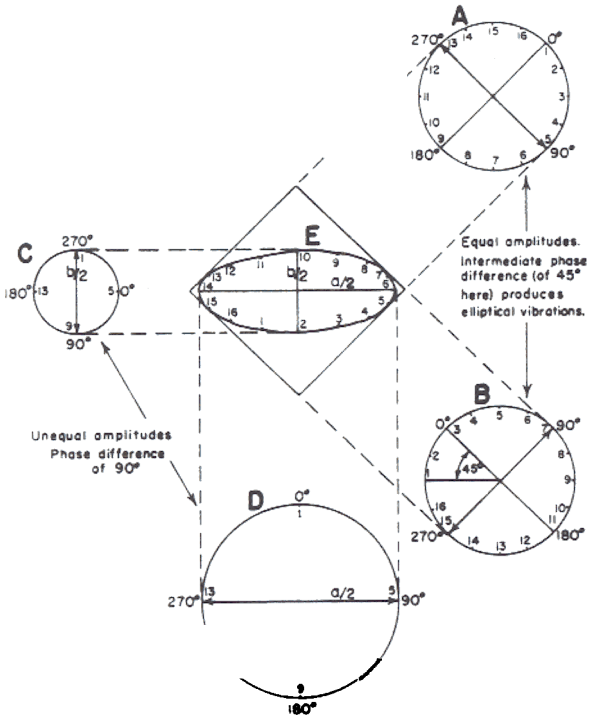

Figure 6. — Production of the same ellipse either by two rays of equal amplitude and intermediate phase difference or by two rays of unequal amplitude (a/2 and b/2) and phase difference of 90 degrees.

Each section is placed in the polarizing microscope (equipped with the compensator). The wall layer is positioned with its vibration directions 45° to those of the polarizer and analyzer (and to the compensator). The analyzer is rotated until the layer becomes dark. The rotation angle is α in the birefringence equation. Whether the analyzer is rotated clockwise or counterclockwise depends on whether the slow (*E*) or fast (*O*) ray of the wood has been positioned counterclockwise to the slow ray of the compensator. In wood the slow ray vibrates parallel to the long axis of the microfibrils and the fast ray perpendicular to them.

The section thickness is required to determine the birefringence[2,5]. It may be obtained after the above measurements have been made by staining the section, embedding it in polyethylene glycol 1540, and resectioning. The thicknesses may be measured with a microscope equipped with an eyepiece filar micrometer.

The average birefringence for each cell wall layer is plotted against the section angle, and a curve is fitted to the points. The peak of the curve locates the section that would be parallel to the microfibril orientation of that layer, and consequently indicates the fibril angle.

FPRS Wood Award Paper . . .

Tension Wood Anatomy of Silver Maple

By

Floyd G. Manwiller[1]

Southern Forest Experiment Station

New Orleans, La.

HARDWOOD TREES of many species form tension wood on the upper side of branches and leaning stems. This reaction tissue is characterized by fibers containing an internal unlignified gelatinous layer. Other layers of the cell wall may or may not have reduced lignification.

Tension wood differs from normal in many aspects, one of the most important being its excessive longitudinal shrinkage during drying. Consequently, when tension wood occurs in the same piece with normal tissue, differential shrinkage often causes warping and splitting.

The explanation for the abnormal behavior of the tension wood tissue must ultimately be found in the chemical and physical organization of the cell wall. In the study reported here, the objective was to determine, through use of the polarizing microscope: 1) the layering sequence, 2) layer thickness, and 3) layer fibril angle in the radial cell walls of both normal wood and tension wood of silver maple (*Acer saccharinum* L.). Specifically, normal fibers from a nonleaning tree were compared with gelatinous and nongelatinous fibers from the tension-wood zone of trees leaning 10° and 20°.

Silver maple, a fast growing bottom-land species, is phototropic and therefore characterized by leaning stems. Tension wood in the species is consequently so abundant as to be of considerable concern to commercial users.

The normal wood fiber consists of a primary wall and a secondary wall of three layers: S_1, S_2, and S_3 (Figure 1). The layers contain a system of helically wound microfibrils. If, in the wall nearest the observer, the helix spirals upward to the right, it is termed a Z helix, and if upward to the left, an S helix. Helix steepness is measured by the fibril angle (Figure 1). The primary wall consists of microfibrils with a loose, feltlike appearance. The S_1 and S_3 layers are composed of

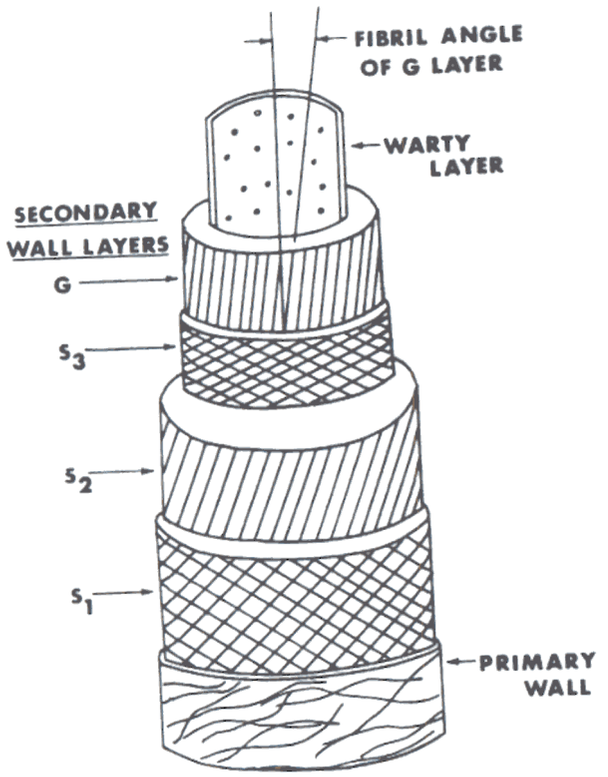

Figure 1. — Cell wall of a hardwood fiber, with all possible layers depicted.

ner.

Electron micrographs showed that G layers of cells from both leaning trees contained the typical honeycomb structure and terminal lamella.

[1]The research was conducted while the author was Research Associate at Iowa State University. Journal Paper No. J-5365 of the Iowa Agriculture and Home Economics Experiment Station, Ames, Iowa, Project 1583.

lamellae of alternating S and Z helices with relatively large fibril angle, while the S_3 lamellae normally display steep Z helices of uniform fibril angle. A thin transition zone of changing fibril angle occurs between the S_1 and S_2 layers and between the S_2 and S_3. Finally, an isotropic warty layer may be present next to the lumen.

In tension wood, a gelatinous (G) layer may replace one or more of the secondary wall layers or be present in addition to them. The gelatinous layer is highly crystalline with steep fibril angle, unlignified, and poorly bound to the rest of the cell wall.

Procedure

During the winter of 1964-65, samples were taken from three silver maple trees. One was straight and nonleaning, one leaned 10° from the vertical at breast height, and the third leaned 20°. Environmental factors were assumed to be constant since the trees were growing together on the same aspect, were all about 45 years old and of the same size, and had approximately the same position in the crown cover.

A single breast-height specimen was taken from the upper side of the leaning trees and at random in the nonleaning tree. Specimens measured approximately 10 centimeters longitudinally, 5 centimeters tangentially, and 2 centimeters radially. Each was notched to record its orientation in the tree and then submerged in water and refrigerated until used.

Fibril angles were determined from birefringence measurements made on a polarizing microscope equipped with a Senarmont compensator (10). Preliminary research showed that the microfibrils of the S_3 and G layers had Z orientations. Layer fibril angles were to be determined in the left radial walls of the cells, facing outward from the pith. The section angles, therefore, were laid out on that wall, sloping downward toward the pith. Each specimen was divided into 10 small microtome blocks whose sectioning surfaces varied from transverse to longitudinal in approximately 10° increments. A corner (the same each time) was removed from each block with a full-length longitudinal bevel cut. The orientation in the tree of each subsequent microtome section was indicated by the missing corner. To avoid inherent variation, the observations were confined to cells of the earliest one-fourth of the ring for 1963, a year of normal growth.

In polarized light, cell wall layers appear light or dark, in accordance with their microfibril orientation, and are thus distinguishable (10). Thick or damaged sections cause light scattering that makes light layers appear wider at the expense of dark ones. To make it possible to cut sections 5 to 10 microns thick and to keep the G layer in position, the blocks were softened and embedded. Softening was accomplished by boiling 1-1/4 hours in 1 part glacial acetic acid to 4 parts 3-percent hydrogen peroxide. After a 4-hour wash, the blocks were embedded at 55°C. in polyethylene glycol 1540 to stabilize the green dimension (first in PEG 1000 for 4 hours, then in PEG 1540 for 4 hours). A vacuum was pulled periodically to increase penetration.

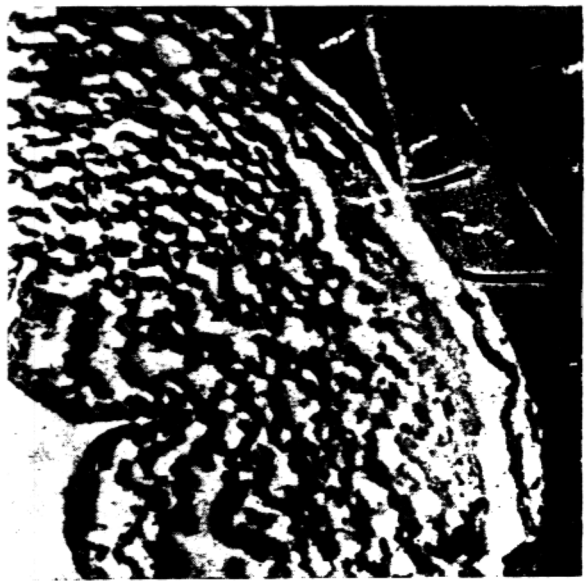

Figure 2. — Transverse section of portion of gelatinous fiber from tree of 20° lean. Terminating layer and honeycomb structure of G layer visible. Green specimen. Embedded in methacrylate. 12,425 X

After the desired sections had been cut, one thin longitudinal slice was removed from each block's radial face with a razor blade. On this slice, 10 determinations of sectioning angle were made in a microscope with an angle-measuring eyepiece.

For birefringence and thickness observations, the microtome sections were mounted unstained in water, which dissolved the polyethylene glycol. Birefringence measurements were made on 20 cells in each section from the nonleaning tree, and on 20 nongelatinous and 20 gelatinous fibers in each section from the two leaning trees.

In the radial wall of each cell measured, a birefringence determination was made on each secondary wall layer (at 1000X). A wavelength of 0.546 micron was obtained by filtering the regular tungsten light source. The birefringence equation (10) was then:

$$\text{Birefringence} = \frac{\alpha\ (0.000083)}{d}$$

where α is the amount of analyzer rotation, in degrees, required for the cell wall layer to become dark, and d is the section thickness in microns. Thickness was the average of 10 measurements on each section. The section was stained with hemalum and embedded in PEG 1540, then resectioned with a razor blade. The resections were measured under a microscope equipped with an eyepiece filar micrometer.

Cell layer thicknesses were measured on the transverse sections used in the birefringence determinations.

The relative proportion of gelatinous to nongelatinous fibers was determined for the leaning trees. Green untreated sections were stained with chloriodide of zinc to make the G layer more visible and then projected at 430X onto a grid developed by Arganbright (1) for determination of the proportions of fibers.

Results

The tree leaning 20° contained greater concentrations of gelatinous fibers than did the 10° tree, and these fibers differed from those of the 10° tree in layering sequence, fibril angles, and some layer thicknesses.

Eighteen percent of the fibers were gelatinous in the 10° tree, and 48.5 percent were gelatinous in the 20° tree. Berlyn (3) found that in cottonwood there is a positive correlation between the degree of lean and the concentration of gelatinous fibers.

Some specimens were embedded green for electron microscopy. The embedding medium was methacrylate, which during polymerization expands the G layer to reveal its structure. The G layer in specimens from both leaning trees showed the honeycomb structure observed by Casperson (4), Cote and Day (5), and Sachsse (15) and the thin terminal lamella observed by Cote and Day and Sachsse (Figure 2). Figure 3 indicates that the microfibrils are common to more than one lamella. A warty layer could not be observed with either the electron or polarizing microscopes. Liese (9) reports, however, that a warty layer is present in all species studied so far in Aceraceae and that it occurs in tension wood cells.

The layering sequence of the 20° tree was S_1, S_2, S_3, G, while the gelatinous fibers of the 10° tree had no S_3 layer. Onaka (11) and Wardrop and Dadswell (20) have found layer sequences of (*a*) S_1, G; (*b*) S_1, S_2, G; and (*c*) S_1, S_2, S_3, G. Onaka (11) stated that tension wood of each hardwood family is characterized by a specific layering sequence. Wardrop and Dadswell, however, found type *a* in the early wood of *Eucalyptus gigantea* and type *b* in the late wood. The current study also indicates that there is more than one layering sequence in a species.

Figure 3. — Longitudinal section of G layer from tree of 10° lean. Green specimen. Embedded in methacrylate. 12,425 X

Table 1. — COMPARISON[1] OF LAYER THICKNESSES IN CELL RADIAL WALLS

PRIMARY + S_1 LAYER					
Cell type[2]	10°, NG	10°, G	20°, NG	20°, G	0°
Thickness, microns	0.32	0.41	0.45	0.50	0.51
S_2 LAYER					
Cell type[2]	20°, G	10°, NG	0°	20°, NG	10°, G
Thickness, microns	1.01	1.06	1.40	1.42	1.74
S_3 LAYER					
Cell type[2]	20°, G	10°, NG	20°, NG	0°	
Thickness, microns	0.31	0.34	0.34	0.48	
G LAYER					
Cell type[2]	10°, G	20°, G			
Thickness, microns	0.78	1.40			
TOTAL WALL					
Cell type[2]	10°, NG	20°, NG	0°	10°, G	20°, G
Thickness, microns	1.72	2.21	2.39	2.93	3.22

[1]Duncan's (1955) multiple range test. Any two values not joined by a line are significantly different at the 99-percent confidence level.

[2]0°, 10°, or 20° indicates degree of tree lean at breast height; G indicates gelatinous fibers, and NG nongelatinous fibers from the reaction zone.

In cells of the 20° tree, the G layer averaged 1.40 microns in thickness (Table 1) and was nearly always at least partially separated from the rest of the cell wall in spite of the care taken in cutting the embedded specimens. In contrast, the G layer of the 10° fibers was thin (0.78 micron) and usually remained in place. At magnifications below 1000X in unpolarized light the gelatinous fibers of the 10° tree could not be distinguished from nongelatinous ones.

In both gelatinous and nongelatinous fibers of the leaning trees, the S_3 layer, when present, was thinner (0.31 to 0.34 micron) than in fibers from the nonleaning tree (0.48 micron). The S_2 layer, which in normal cells is typically variable in thickness, was erratic with no trends (1.01 to 1.74 microns). The primary and S_1 layers were measured as one since they are not distinguishable in polarized light. The P + S_1 layers of normal fibers were not significantly (0.05 level) thicker (0.51 micron) than those of the gelatinous and nongelatinous fibers of the 20° tree (0.50 and 0.45 micron), but were significantly thicker when com-

pared with those of the 10° tree (0.41 and 0.32 micron). The S_1 layer of gelatinous fibers often appears thinner than that of normal fibers (18).

The values of Table 1 do not necessarily represent true layer thicknesses, since in the polarizing microscope one sees only the optical effects of the different fibrillar orientations. In the few measurements available with the electron microscope, the primary + S_1 and the S_3 layers were thinner than averages for the comparable layers measured with polarizing microscope.

Figure 4 shows one set of birefringence curves, those for the wall layers of the gelatinous fibers of the 20° tree. The plotted data for the S_1 and S_3 layers usualy had a relativey smooth form with the major maximum inflection point near the center of the range of X. A second maximum was present between 0° and 12° for each layer; the cause is uncertain—it may be a reflection of the transition zone between the S_1 and S_2 layers and between the S_2 and S_3. Mark also found this second maximum (10a).

To obtain the fibril angle, the second-degree polynomial

$$Y = B_0 + B_1X + B_2X^2$$

was fitted by the method of least squares regression (16) to a part of the range of birefringence observations, Y_i, and associated section angle, X_i, for each curve. A second-degree polynominal could not be expected to fit well where more than one inflection point occurred, but in the region of the maximum, where it would fit well, it offered the possibility of constructing confidence limits. Therefore, the maximum point was determined by differentiation with respect to X. When the derivative

$$\frac{dy}{dx} = 0 + B_1 + 2B_2$$

was set equal to zero and solved for x, the fibril angle was obtained. The ranges of X and number of points, n, over which the polynomial was fitted for each layer are given in Table 2.

The fibril angles of the S_1, S_2, and S_3 layers of both gelatinous and nongelatinous fibers of the leaning trees were, with one exception, similar to or greater than the corresponding angles for the nonleaning tree. The S_1 fibril angles of the leaning trees ranged from 45° to 51° as compared to 44° for normal fibers. The S_3 fibril angle was 5° for the nongelatinous fibers of the 10° tree; the remaining S_2 fibril angles of the leaning trees were from 11° to 25° as compared to 12° for normal fibers. Wardrop and Dadswell (19) estimated the S_1 and S_2 fibril angles to be somewhat less in gelatinous fibers than in normal cells. The angles for the S_3 layer of gelatinous and nongelatinous fibers, when this layer was present, were larger (26° to 29°) than in normal fibers (20°).

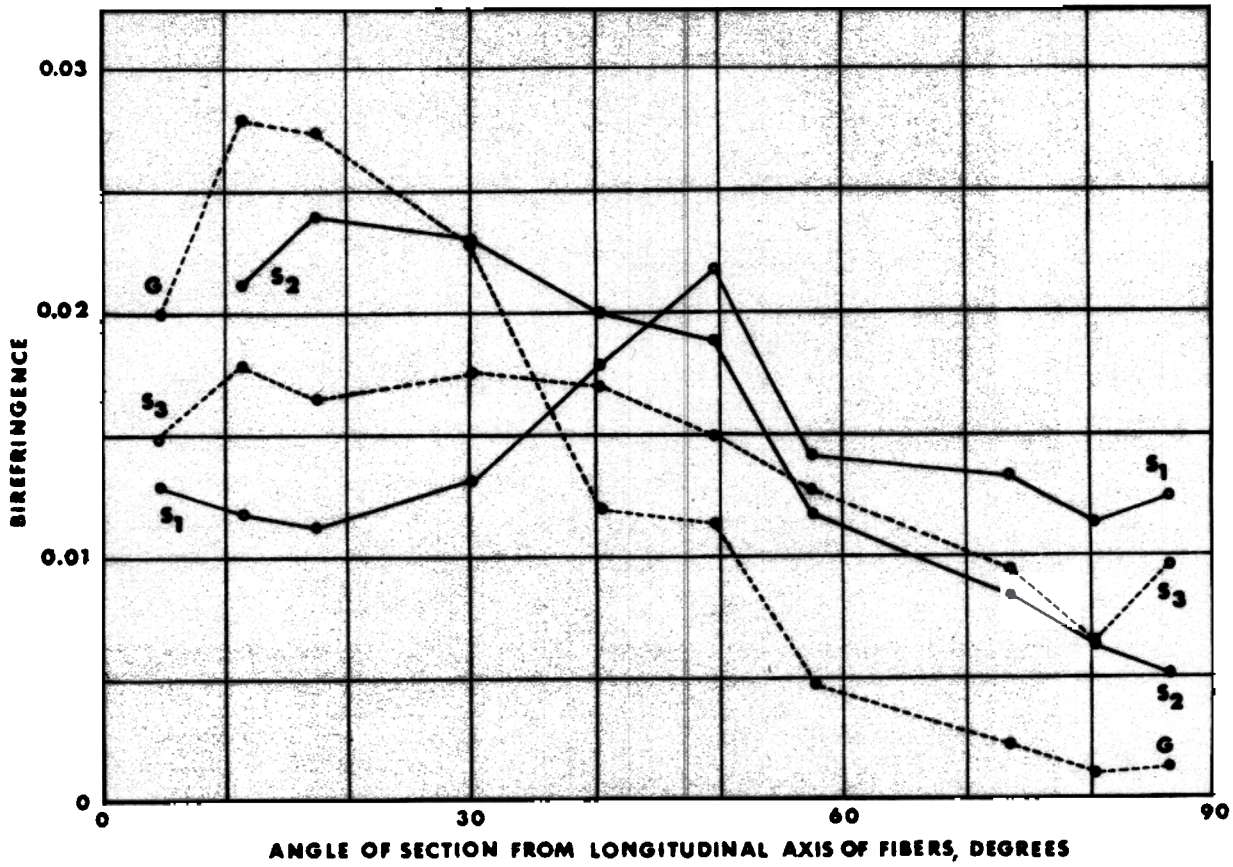

Figure 4. — Birefringence for gelatinous fibers from tree of 20° lean. Each point represents the [illegible] of one observation on each of 20 cells.

Table 2. — CALCULATED FIBRIL ANGLES IN LAYERS OF CELL RADIAL WALLS

Layer	Nonleaning tree normal fibers			Tree leaning 10°						Tree leaning 20°					
				Gelatinous fibers			Nongelatinous fibers			Gelatinous fibers			Nongelatinous fibers		
	No. of points	Range of x	Fibril angle	No. of points	Range of x	Fibril angle				No. of points	Range of x	Fibril angle	No. of points	Range of x	Fibril angle
	n	Deg.	Deg.	n	Deg.	Deg.	n	Deg.	Deg.	n	Deg.	Deg.	n	Deg.	Deg.
S_1	7	9-71	44	5	20-66	45	4	29-66	45	7	17-80	49	7	17-80	51
S_2	7	4-61	12	7	5-66	12	5	5-43	5	6	12-58	25	10	5-86	
S_3	7	9-71	20	5	20-66	—	5	20-66	29	7	17-80	26	5	17-58	29
G	—	—	—	5	5-43	8	—	—	—	7	5-58	15	—	—	—

NOTES: Calculated fibril angles based on the second degree polynomial fitted by least squares regression (Snedecor, 1956, pp. 414-416, 452-455) to the quadratic portion of the data; the number of points, n, over which the polynomial was fitted; the range of x (to nearest degree) over which the polynomial was fitted.

The G layer of the 10° tree had a fibril angle of 8°, comparable to the 5° to 8° reported by Wardrop and Dadswell (19), but that of the 20° tree (15°) was greater than has been reported. Preston and Ranganathan (14), Wardrop and Dadswell (20), and Cote and Day (5), without measuring it, have estimated the G layer fibril angle to be almost axial.

Fuller's (8) method was used to calculate a confidence limit for the true fibril angle, X_{max}. The interval, at 95-percent confidence coefficient, is:

$$\frac{B_1 - t_{0.05,n-3}\sqrt{s^2 D(X'X)^{-1}D'}}{2B_2} \leq X_{max} \leq \frac{B_1 + t_{0.05,n-3}\sqrt{s^2 D(X'X)^{-1}D'}}{2B_2}$$

where $t_{0.05,n-3}$ = value of Student's t for 95-percent confidence coefficient and n-3 degrees of freedom

s^2 = residual mean square about regression

B_1 = partial regression coefficient for X

B_2 = partial regression coefficient for X^2

D = a 1 x 3 matrix of the terms in $\frac{dy}{dx} = (0\ B_1\ 2B_2)$

D' = transpose of D

X = an n x 3 matrix of observations of X_1 with the first row being $(1\ X_1\ X_1^2)$ for observation set 1

X' = transpose of X

$(X'X)^{-1}$ = inverse of the $(X'X)$ matrix, i.e., the inverse of the matrix of sum of squares and products of X uncorrected for the means.

The attempt to determine confidence intervals was only partially successful. Several of the S_1 and S_2 fibril angles had an interval of ±3°. In general, however, an insufficient number of points resulted in a poor estimate of s^2 and in a large t value. In addition, the points for the S_3 and G layers were unbalanced, with only one or two points to the left of the maximum. The confidence intervals for these layers, therefore, were often extremely wide (±34° for the G layer of the 20° tree, for example). This kind of variability is not indicated by the fibril angles obtained in this study or in other observations made on tension wood.

Discussion

When wood dries, shrinkage occurs at right angles to the length of the microfibrils. In normal wood, longitudinal shrinkage from green to oven-dry is only about 0.1 to 0.3 percent, because the thick S_2 layer with its steep fibril angle dominates the other layers. Despite the additional G layer with its steep fibril angle, tension wood has abnormally high longitudinal shrinkage, with values up to 1.55 percent; the shrinkage increases as the concentration of gelatinous fibers increases (2, 13, 17). The results of this study indicate that not only are there greater numbers of abnormal fibers at the greater lean, but that the individual fiber is more prone to longitudinal shrinkage.

In the 10° tree, however, fibril angles and layer thicknesses are not the explanation for abnormal shrinkage. In the gelatinous fibers, the fibril angles of the S_1 and S_2 layers were similar to those of normal cells. Any component of longitudinal shrinkage normally attributed to the S_1 and S_2 layers would be reduced because the P + S_1 layers were thinner than normal and the S_2 was missing. The S_2 layer, which restrains longitudinal shrinkage, was reinforced by its greater thickness and by the G layer, which seemed to be better attached to the rest of the wall than is usual. The steep S_3 fibril angle (5°) of the nongelatinous fibers would further restrict longitudinal shrinkage.

The gelatinous fibers of the 20° tree would have increased longitudinal shrinkage—if the G layer

were assumed not to be attached to the rest of the wall during drying. The fibril angles of the S_1 and the thinner S_3 layers were greater than those of the normal fibers and, more important, the fibril angle of the thick S_2 layer was 25°, as contrasted with 12° for the S_2 of the normal fibers. Similarly, the fibril angles of the nongelatinous S_1 and S_3 layers were larger than normal. Nevertheless, it is doubtful that the results obtained here would explain the 5- to 10-fold increase in shrinkage caused by tension wood. The 25° fibril angle of the S_2 layer is still within the range of 10° to 30° reported for the S_2 of normal fibers (12) and the modifications of the other wall layers are not that great.

The explanation for the shrinkage of tension wood is probably similar to that hypothesized by Wardrop and Dadswell (19, 20) and Dadswell and Wardrop (6) to explain irreversible collapse. A microfibril contains long cellulose molecules whose longitudinal axes are parallel to that of the microfibril. The cellulose molecules are held tightly together along much of their length by hydrogen bonding to form a crystalline core in the microfibril. The paracrystalline sheath surrounding the core is composed of noncellulosic polysaccharides with much less order. As water molecules in the sheath leave during drying, the component molecules move closer together to produce transverse shrinkage. The crystalline core virtually prevents longitudinal shrinkage. Lignin, located in the paracrystalline sheath, is a natural dimensional stabilizer, and its absence from the G layer and often from other layers would permit greater movement of the wall components. The paracrystalline sheath with its low degree of order would have a large longitudinal shrinkage component which could be expressed in the absence of lignin. Also, the lack of lignin would allow greater hydrogen bonding among cell wall polysaccharides when they approach each other during drying. Sachsse (15) found that the G layer of his air- and ovendried specimens were compact and did not show the honeycomb structure of the green specimens. This would indicate that internal bonding had occurred.

Literature Cited

1. Arganbright, D. G. 1964. The occurrence and shrinkage characteristics of tension wood in soft maple. Master's thesis. Library, Iowa State Univ. Sci. and Tech. Ames, Iowa.
2. Baudendistel, M. E., and V. Akins. 1946. High longitudinal shrinkage and gelatinous fibers in an eccentric cottonwood log. Jour. For. 44: 1053-1057.
3. Berlyn, G. P. 1961. Factors affecting the incidence of reaction tissue in *Populus deltoides* Bartr. Iowa State Jour. Sci. 35(3): 367-424.
4. Casperson, G. 1961. Über die Bildung von Zellwänden bei Laubhölzern. 2. Mitteilung. Der zeitliche Ablauf der Sekundärwandbildung. Zeitschrift für Botanik 49(3): 289-306.
5. Cote, W. A., Jr., and A. C. Day. 1962. The G layer in gelatinous fibers—electron microscopic studies. For. Prod. Jour. 12: 333-338.
6. Dadswell, H. E., and A. B. Wardrop. 1956. The importance of tension wood in timber utilization. Aust. Pulp and Paper Ind. Tech. Assoc. Proc. 10: 30-42.
7. Duncan, D. B. 1955. Multiple range and multiple F tests. Biometrics 11: 1-42.
8. Fuller, W. A. 1962. Estimating the reliability of quantities derived from empirical production functions. Jour. Farm Econ. 44(1): 82-99.
9. Liese, W. 1965. The warty layer. In Cote, W. A., Jr., ed. Cellular ultrastructure of woody plants, pp. 251-270. Syracuse Univ. Press. Syracuse, New York.
10. Manwiller, F. G. 1966. Senarmont compensation for determining fibril angles of cell wall layers. For Prod. Jour. 16(10): 26-30.

10a. Mark, R. 1965. Tensile stress analysis of cell walls of coniferous tracheids. In Cote, W. A., Jr., ed. Cellular ultrastructure of woody plants, pp. 493-533. Syracuse Univ. Press. Syracuse, N. Y.

11. Onaka, F. 1949. Studies on compression and tension wood. Wood Res. Inst., Kyoto, Bull. No. 1.
12. Panshin, A. J., C. De Zeeuw, and H. P. Brown. 1964. Textbook of wood technology. Ed. 2. McGraw-Hill Book Co. New York, N. Y.
13. Pillow, M. Y. 1950. Presence of tension wood in mahogany in relation to longitudinal shrinkage. U.S. Dept. Agric. For. Prod. Lab. Rept. No. D1763.
14. Preston, R. D., and V. Ranganathan. 1947. The fine structure of the fibers of normal and tension wood in beech (*Fagus sylvatica* L.) as revealed by X-rays. Forestry 21: 92-98.
15. Sachsse, H. 1962. Electronemikroskopische Untersuchungen uber die Zellwandstruktur von Zugholzfasern. Holz als Roh- und Werkstoff 20: 429-433.
16. Snedecor, G. W. 1956. Statistical methods. Iowa State Univ. Press. Ames, Iowa.
17. Wahlgren, H. E. 1957. Tension wood in overcup oak. U.S. Dept. Agric. For. Prod. Lab. Rept. 2089.
18. Wardrop, A. B. 1964. The reaction anatomy of arborescent angiosperms. In Zimmerman, Martin H., ed. The formation of wood in forest trees, pp. 405-456. Academic Press. New York, N. Y.
19. ————, and H. E. Dadswell. 1948. The nature of reaction wood. I. The structure and properties of tension wood fibres. Aust. Jour. Sci. Res. Series B, Biol. Sci. 1(1): 3-16.
20. ————, and H. E. Dadswell. 1955. The nature of reaction wood. IV. Variations in cell wall organization of tension wood fibres. Aust. Jour. Bot. 3: 177-189.

Publisher: Forest Products Research Society
417 N. Walnut St., Madison, Wis. 53705